Accepted Manuscript

Plasma-induced PAA-ZnO coated PVDF membrane for oily wastewater treatment: Preparation, optimization, and characterization through Taguchi OA design and synchrotron-based X-ray analysis

Xiujuan Chen, Gordon Huang, Chunjiang An, Renfei Feng, Yinghui Wu, Charley Huang

PII: S0376-7388(19)30362-X

DOI: https://doi.org/10.1016/j.memsci.2019.03.091

Reference: MEMSCI 16993

To appear in: *Journal of Membrane Science*

Received Date: 1 February 2019

Revised Date: 18 March 2019

Accepted Date: 30 March 2019

Please cite this article as: X. Chen, G. Huang, C. An, R. Feng, Y. Wu, C. Huang, Plasma-induced PAA-ZnO coated PVDF membrane for oily wastewater treatment: Preparation, optimization, and characterization through Taguchi OA design and synchrotron-based X-ray analysis, *Journal of Membrane Science* (2019), doi: https://doi.org/10.1016/j.memsci.2019.03.091.

Plasma-induced PAA-ZnO Coated PVDF membrane for oily wastewater treatment: preparation, optimization, and characterization through Taguchi OA design and synchrotron-based X-ray analysis

Xiujuan Chen[a], Gordon Huang[a,*], Chunjiang An[b], Renfei Feng[c], Yinghui Wu[a], Charley Huang[d]

[a] Faculty of Engineering and Applied Science, University of Regina, Regina, Saskatchewan, Canada S4S 0A2

[b] Department of Building, Civil and Environmental Engineering, Concordia University, Montreal, Quebec, Canada H3G 1M8

[c] Canadian Light Source, Saskatoon, S7N 2V3, Canada

[d] Department of Chemical and Materials Engineering, University of Alberta, Edmonton, Alberta, Canada T6G 1H9

*corresponding author, phone: +1-306-585-4095; fax: 1-306-585-4855; e-mail: huangg@regina.ca

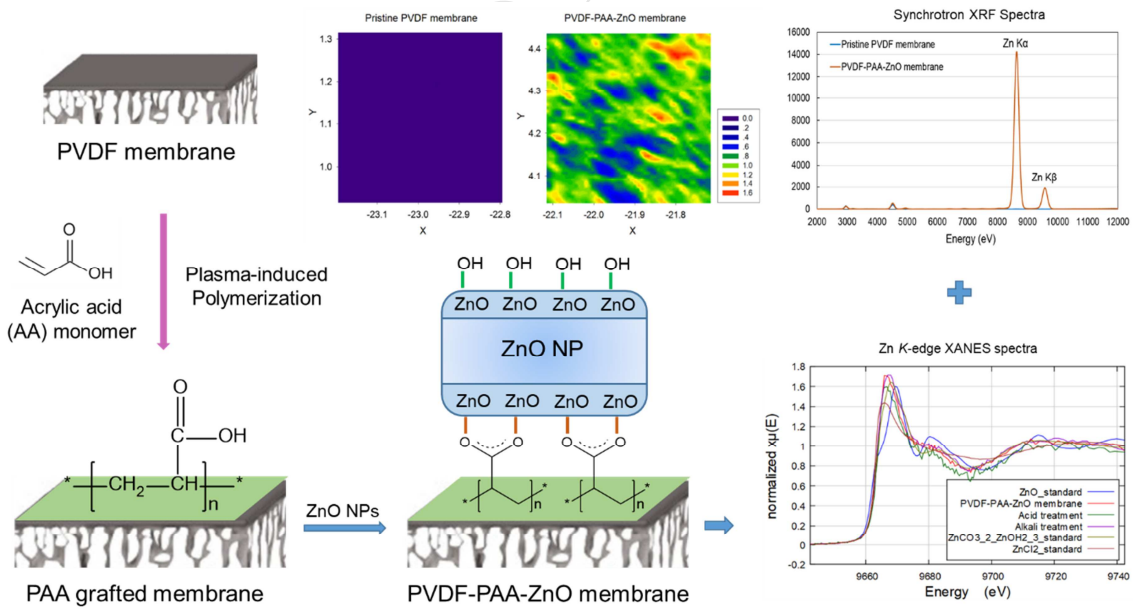

Abstract art

ABSTRACT: A novel membrane surface modification approach was proposed to successfully obtain a poly(vinylidene fluoride)-poly(acrylic acid)-ZnO (PVDF-PAA-ZnO) membrane with super-high water permeability and great oil rejection through cold plasma-induced PAA graft-polymerization followed by simple nano-ZnO self-assembly. The experimental parameters of modification were optimized and their optimal combination was identified using Taguchi OA design method. The PVDF-PAA-ZnO membrane was comprehensively characterized and the mechanism of nano-ZnO self-assembly was explored by contact angle measurement, scanning electron microscope (SEM) images, elemental analysis, tension test, Attenuated Total Reflection-Fourier Transform Infrared Spectroscopy (ATR-FTIR) and synchrotron-based X-ray analyses. It was revealed that ZnO NPs were immobilized onto membrane surface through the adsorption of PAA layer to form a PAA-ZnO coating without valence change. The carboxyl groups of PAA layer provided complexing ligands to coordinate with Zn^{2+} and form bidentate species on the nano-ZnO surface. The firm PAA-ZnO coating on PVDF membrane surface converted its hydrophobic nature to hydrophilic, bringing about the dramatically improvement of membrane performance both in water permeation flux and oil rejection rate. The permeation flux of the PVDF-PAA-ZnO membrane was more than 10 times as great as that of the pristine PVDF membrane.

Keywords: Taguchi orthogonal array (OA) design, plasma-induced PAA polymerization, nano-ZnO self-assembly, synchrotron-based X-ray analysis

1. INTRODUCTION

Increasing oily wastewater pollution caused by petrochemical activities such as onshore/offshore oil recovery and marine transportation have brought about serious health risks and the destruction of ecosystems, becoming an urgent global environmental problem [1, 2]. The development of effective methods for oily wastewater treatment is desired and full of challenges, particularly for the separation of oil/water emulsions [3, 4]. Most of the traditional techniques, such as gravity separation, flocculation and flotation, suffer from low efficiency, high cost, and secondary pollution [5-9]. Polymer filtration

membranes have been frequently applied in practical applications of oily wastewater treatment owing to their lower cost and ready availability [10, 11]. Among them, polyvinylidene fluoride (PVDF) membranes are extensively used due to its outstanding mechanical properties, thermal stability, and chemical resistance [12]. Nevertheless, they still encounter two main limitations which affect their separation efficiency and operating cost. Firstly, both water and oil are adsorbed on membrane surfaces during the treatment process because of their poor separation selectivity. Secondly, serious pore clogging and surface fouling is caused by oil or grease, leading to a recessive reduction in permeate flux.

To address these two limitations, a number of advanced PVDF membranes have been developed by various modification techniques with the incorporation of nanoparticles (NPs) to improve the membrane hydrophilicity and antifouling ability. Many types of NPs have been utilized in membrane modification, such as iron (Fe^0, Fe_2O_3, Fe_3O_4), silica dioxide (SiO_2), alumina (Al_2O_3), titanium dioxide (TiO_2), zirconium dioxide (ZrO_2), carbon nanotubes, graphene oxide, etc. [13-17]. For example, the incorporation of TiO_2 NPs in membrane modification as an additive in the polymer matrix or immobilized on the membrane surface has been widely studied [18, 19]. Alternatively, zinc oxide (ZnO) NPs have been applied as a replacement for TiO_2 NPs since they have similar properties but the crystal form of nano-ZnO is easier to control and the price is slightly lower [20-22]. Hence, ZnO NPs have attracted an increasing amount of interest in membrane modification to improve the performances of PVDF membranes. Hong and He (2012) reported a composite PVDF-ZnO membrane that exhibited improved mechanical properties and BSA (blood serum albumin) rejection by adding 0.1% nano-ZnO particles into the casting solution. The highest pure water flux of the composite PVDF membrane was achieved when the supplemental nano-ZnO content was increased to 1.5%, and it was nearly five times higher than that of a pristine PVDF membrane [23]. Liu et al. (2016) prepared electrospun PVDF membranes with controllable structures and tunable wettability for oil/water separation. The membrane with a maximum water contact angle of 171 $\pm$ 1.5° was obtained by adding 8 wt% ZnO NPs into the polymer matrix [24]. Liang et al. (2012) modified PVDF membranes for synthetic municipal wastewater treatment by blending ZnO NPs in its cast solution to

improve the anti-irreversible fouling properties. The water permeability was almost doubled when the dosage (6.7% nano-ZnO) was added [20].

However, most of previous research on ZnO NPs for PVDF membrane modification was limited to blending ZnO NPs into the casting solution. The improvements of membrane properties such as hydrophilicity and fouling resistance were restricted by doing so. The modification efficiency was affected because the ZnO NPs agglomerated in the casting solution, causing them to be entirely enfolded by the polymer matrix. In comparison, immobilizing ZnO NPs on the membrane surfaces using techniques of coating or chemical grafting to form a stable functional layer could be a more effective modification approach. Most of the ZnO NPs can disperse on PVDF membrane surfaces to maximally improve their performances. The challenge of this approach is how to stably immobilize ZnO NPs on the membrane surface, since ZnO NPs cannot self-assemble onto PVDF membrane surface without bonding with suitable functional groups.

Herein, a novel membrane surface modification approach was proposed to obtain a PVDF-PAA-ZnO membrane which was modified from PVDF membrane through cold plasma-induced poly(acrylic acid) (PAA) graft-polymerization followed by simple nano-ZnO self-assembly. The technique of cold plasma surface treatment was applied to induce PAA polymerization by introducing chemical initiators on PVDF membrane surface. An ultrathin and uniform PAA layer can thus be formed on the membrane surface to realize nano-ZnO self-assembly without compromising the bulk structure. To maximize the improvement of membrane hydrophilicity, the Taguchi orthogonal array (OA) design was applied to optimize the experimental parameters and identify their optimal combination. The obtained PVDF-PAA-ZnO membrane was comprehensively characterized and the mechanism of nano-ZnO self-assembly was explored by contact angle measurement, scanning electron microscope (SEM) images, elemental analysis, tension test, attenuated total reflection-Fourier transform infrared spectroscopy (ATR-FTIR), and synchrotron-based X-ray analyses. The PVDF-PAA-ZnO membrane was subjected to physical and chemical stresses to evaluate the binding performance of the PAA-ZnO coating. The improvement in membrane performance was further assessed for the application of oily wastewater treatment.

2. MATERIALS AND METHODS

Materials and chemicals. The PVDF membrane used in this study has an average pore size of 0.1 μm, commercially available from TQX Membrane Technology Ltd. (Xiamen, China). Before modification, the PVDF membranes were soaked in DI water and underwent ultrasonic treatment at 250 W, 40 KHz for 5 minutes to remove preservative materials, and then dried in air. ZnO NPs (< 100 nm) were purchased from Innochem (Beijing, China). Diesel was a commercial product purchased from Shell gas station (Regina, Canada). All other chemicals were purchased from Sigma-Aldrich (MilliporeSigma Canada Co., Oakville, Canada) with analytical grade, and used as received without further purification.

Preparation of PVDF-PAA-ZnO membrane. The commercial PVDF membrane was cut into a 7.5 cm × 5.8 cm flat sheet, and the flat sheet was placed in the chamber of the gas plasma treatment system (IoN 40, PVA TePla, USA) with only the membrane surface exposed, as shown in Figure S1. After the chamber was evacuated, Ar gas was injected into the chamber and the flow rate was maintained at 300 sccm. Plasma was generated by radio frequency with 125 W of power for irradiation under Ar gas environment, and the pressure in the chamber was stable at 970 ± 10 mTorr. Then the chamber was evacuated again to eject Ar, and O_2 gas was injected to generate free radicals on the membrane surface. After plasma treatment, the membrane was immersed in AA solution for PAA graft polymerization. A water bath was used to maintain the temperature of PAA graft polymerization at 70 ^{o}C during the designated period. After PAA graft polymerization, the membrane was rinsed three times to remove unreacted AA monomers and unstable PAA homopolymers. Next, the PAA-grafted membrane was immersed into ZnO NPs suspension for 1 hour to let ZnO NPs self-assemble, and then dried at 20 ^{o}C for 1 hour. Finally, the membrane was dipped in DI water and shaken at 300 rpm for 30 min to remove ZnO NPs that were weakly bound, and then the modified membrane was completely dried at 20 ^{o}C to obtain the final PVDF-PAA-ZnO membrane. A visual representation of the entire process of the performed membrane surface modification is presented in Figure 1.

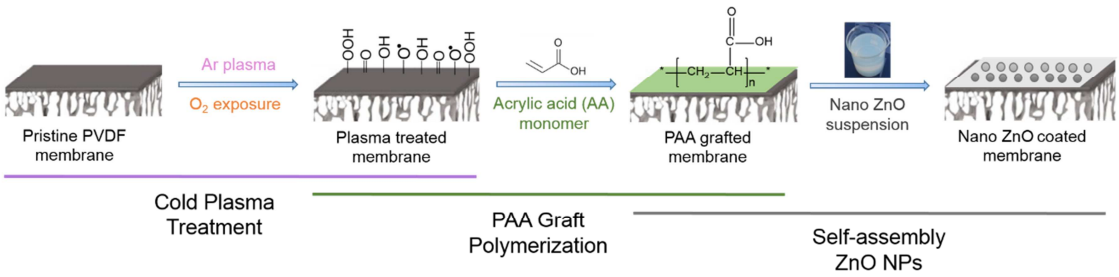

Figure 1: Preparation of the PVDF-PAA-ZnO membrane.

Taguchi orthogonal array (OA) design. Taguchi's optimization technique is a powerful optimization method that has been widely applied in scientific investigations to identify optimal conditions with minimum number of experiments [25, 26]. In this research, the effects of five important factors including A-Ar reaction time, B-O_2 flow rate, C-AA concentration, D-AA reaction time, and E-Nano-ZnO concentration on the hydrophilicity improvement of PVDF membrane were studied using OA design. Table 1 summarizes all the factors and their variable levels in this experiment. An OA16 (4^5) design was employed, and the experimental matrix was generated using Design-Expert v10 (Stat-Ease Inc., Minneapolis, USA). The water contact angle of the membrane surface was applied as the experimental response in the statistical analysis. Water contact angle is widely used to represent the degree of hydrophilicity of membranes. In this study, a smaller water contact angle value would indicate a stronger membrane hydrophilicity because of more efficient modification. There were 16 experiments in total to complete the OA16 (4^5) design, and the experiments under the same conditions were carried out in triplicate to obtain suitable precision. The experiments were carried out randomly to avoid personal or subjective bias. Finally, the water contact angle of the membrane surface modified under the optimized experimental conditions was further measured to validate the OA method.

Table 1: Experimental factors and levels used in this study

Factors	Levels			
A: Ar reaction time (s)	30	60	90	120
B: O_2 flow rate (sccm)	300	350	400	450
C: AA concentration (%, v/v)	55	60	65	70
D: AA reaction time (h)	1.25	1.5	1.75	2

E: Nano-ZnO concentration (mg/L)	1	2	3	4

Characterizations. The morphology observation and elemental investigation of the PVDF membrane surface was carried out using a Scanning Electron Microscope (SEM) equipped with an Energy Dispersive X-ray analysis (EDX) system (JSM-6510, Rigaku, Japan). The FTIR absorption spectra of ZnO NPs, membrane surface, and membrane backside were measured to investigate their chemical compositions using Tensor 27 Attenuated Total Reflection-Fourier Transform Infrared Spectroscopy (ATR-FTIR) (Bruker, Billerica, USA). The standard parameter for data collection was set at 16 scans in the wavenumber range of 400 - 4000 cm^{-1}. The membrane mechanical properties before and after modification were measured by the Model 42 Material Test System (MTS Criterion, Eden Prairie, USA). The membranes were cut into 0.6 cm × 10 cm strips and completely dried before measurement (Figure S2). Each measurement was repeated five times and the average value was reported.

An OCA20 contact angle analyzer (DataPhysics Instruments, Charlotte, USA) was used to determine the contact angle of the membrane surface based on the standard sessile drop method. The measurement of water contact angle was conducted by dropping 5 μL of water from a micro-syringe with a stainless steel needle onto the membrane surface. To determine the underwater oil contact angle, the membrane was fixed and immersed in DI water, and then a 5 μL droplet of diesel oil was dropped carefully onto the membrane surface. The data of contact angle was acquired every 30 ms using CCD camera. The surface energy of the pristine membrane was calculated by using Wu's Harmonic Mean (Wu har) method with DI water and diiodomethane as standard liquids. The surface energy of modified membrane was calculated by using Owens, Wendt, Rabel & Kalble (OWRK) method with two standard liquids which were DI water and Ethylene glycol. All the data of contact angle and surface energy was recorded and analyzed using SCA20 (DataPhysics Instruments GmbH, Filderstadt, Germany). The adopted contact angle was the average value of 5 repeated measurements in different locations. All measurements were carried out at 20 ± 1 °C.

The Synchrotron-based X-ray analyses were performed at the Very Sensitive Elemental and Structural Probe Employing Radiation from a Synchrotron (VESPERS)

beamline of the Canadian Light Source (CLS) in Saskatoon, Saskatchewan, Canada (Figure S3). The spectra of Zn K-edge X-ray absorption near edge structure (XANES) of ZnO NPs were measured in fluorescence mode with a four-element silicon drift detector (Vortex®-ME4, Hitachi), where the energy of incident X-ray was scanned using a double crystal Si(111) monochromator over the range of 9460 eV ~ 9910 eV. The measurements of X-ray fluorescence (XRF) spectra and XRF mappings of ZnO NPs distribution on membrane surfaces were also carried out. In which the polychromatic X-ray beam (pink beam) was used to excite the membrane samples, and the emitted XRF spectra were recorded by the four-element Vortex® silicon drift detector at each pixel of scan. The intensity of the characteristic X-ray peak in these spectra was used to generate elemental distribution map. The mapping area was usually 400 μm × 400 μm in size, and the scanning step-size was set as 8 μm. All the XRF spectra from a mapping area were averaged to obtain the reported XRF spectrum for this sample.

Evaluation of ZnO NPs binding performance. To evaluate the binding performance of ZnO NPs on membsurface, the modified membrane was subjected to physical and chemical stresses. The physical stress was induced through ultrasonic treatment. The modified membrane was immersed in DI water and placed in the water tank of an ultrasonic cleaner for ultrasonic treatment at 250W, 40 KHz for 1 min. As for the chemical stress, the modified membrane was treated with HCl solution (pH = 2) and NaOH solution (pH = 12) for 15 min, respectively, followed by rinsing three times with DI water. For the modified membrane before and after the chemical or physical stress, the ZnO NPs concentration distribution and water contact angle of the membrane surface were measured and compared.

Treatment of oily water. The stable oily water was artificially synthesized by mixing commercial diesel and DI water in the laboratory. The mixture was stirred for 4 h at 2100 rpm for emulsification, then the oily water was stabilized for 24 hours and the floating oil was removed before treatment. The chemical oxygen demand (COD) concentrations of feed and permeate solutions were determined by a COD analyzer (Hach 2800, London, Canada). The oil droplet size distribution in the synthesized oily water was measured using a Malvern particle size analyzer (Mastersizer 3000, Malvern, UK), and the result is presented in Figure S4. After stabilization, the COD concentration of the

oily water was 180 mg/L and the average oil droplet size was 2.73 μm. The performance of the pristine and PVDF-PAA-ZnO membranes including pure water flux and oil rejection were evaluated using CF016 membrane test skid (Sterlitech Corporation, Kent, USA). The test skid is a bench-top cross-flow filtration system (Figure S5) with 20.6 cm^2 of effective membrane area. The pure water flux was tested under 1 bar of pressure. During the period of oily water treatment, the operating pressure was kept at 3 bar, and the permeate flow was measured using an electronic weighing balance (Valor® 1000, OHAUS, Parsippany, USA). All experiments were carried out in recycling mode, which both concentrate and permeate were recycled to the feed tank. The permeation flux (J_w, $L/m^2 \cdot min$) of the membrane can be expressed as [27]:

$$J_w = \frac{V}{A \times \Delta t}$$

where, V denotes the permeate water volume (L), A denotes the effective membrane area (m^2), and Δt denotes the permeation time (min).

The COD removal rate (R, %) of the membrane can be calculated as:

$$R(\%) = \frac{C_f - C_p}{C_f} \times 100$$

where, C_p is the COD concentration in the permeate water (mg/L), and C_f is the COD concentration in the feed water (mg/L).

Data analysis and quality assurance. The Taguchi OA analysis was conducted using Design Expert v10. The FTIR data was collected and processed using the OPUS 7.2 software (Bruker Optics Inc., Billerica, USA). The data of ZnO NPs distribution and XRF spectra were processed using SigmaPlot (Systat Software Inc., San Jose, USA). The XANES spectra data was analyzed through Athena XAS Data Processing. The quality assurance/quality control program was followed to ensure the accuracy and reliability of the collected data. Experiments were carried out for three different membrane samples which were prepared under the same conditions to estimate the general membrane characteristics.

3. RESULTS AND DISCUSSIONS

Taguchi OA design analysis. Taguchi's optimization technique is an effective

method that can handle parameter optimization with a minimum number of experiments [28]. In this research, the main effects of five important factors (A-Ar reaction time, B-O_2 flow rate, C-AA concentration, D-AA reaction time, and E-Nano-ZnO concentration) on the membrane hydrophilicity improvement and their optimum conditions for membrane modification were investigated. The OA16 (4^5) experimental matrix was shown in Table 2, and the mean value of water contact angle corresponding to each factor at different levels (*r*1, *r*2, *r*3, and *r*4) was calculated and presented in Figure 2. During the plasma treatment process, Ar reaction time showed a slightly positive effect on the improvement of membrane hydrophilicity in the initial stage, the water contact angle decreased from 25.78° to 23.48° during the first 90 s. However, this effect turned to negative when the Ar reaction time was extended to 120 s, and the water contact angle increased to 29.35°. The reason may be that more and more peroxides were formed with the slow reaction between the plasma and membrane surface in the first 90 s [29]. Higher peroxide concentration on the membrane surface would result in more PAA graft polymerization, leading to more ZnO NPs attachment [29, 30]. Nevertheless, excessive Ar reaction time might result in unstable peroxides if the reaction time passed its threshold. In comparison, the change of O_2 flow rate did not significantly influence the membrane hydrophilicity, though it was reported that the peroxides were produced on the membrane surface after plasma treatment under Ar gas environment followed by oxygen exposure [31]. It was also speculated that the plasma would be unstable if the pressure was too high in the reaction chamber due to high oxygen concentrations [32]. Thus, high oxygen flow rate should not be adopted to avoid oxygen waste and unstable plasma.

In the process of PAA graft polymerization, the increase of AA concentration and AA reaction time did not help to improve membrane hydrophilicity, and even let to increasing contact angle. Generally, increase in concentration and temperature would enhance reaction chances and molecule kinetic energy for AA monomers, which can facilitate polymerization before reaching a certain limit. This would help to improve ZnO NPs attachment on the membrane surface. However, the PAA polymerization may be too rapid if the concentration and temperature were very high, which would leave less AA monomers to diffuse onto the membrane surface [29]. The increase in contact angle could be attributed to the prevalence of homo-polymerization under the conditions of higher

AA concentration and temperature. As for the factor E-Nano-ZnO concentration, the mean water contact angle obviously decreased from 31.0° to 19.6° with the increase of nano-ZnO concentration from 1 to 4 g/L. The lower contact angle obtained under the condition of higher nano-ZnO concentration was likely attributed to more ZnO NPs being assembled onto membrane surface. The membrane hydrophilicity thus could be significantly improved owing to the hydrophilic property of ZnO NPs.

Table 2: The OA16 (4^5) experimental matrix for optimization of membrane modification

Exp. no.	A: Ar reaction time (s)	B: O_2 flow rate (sccm)	C: AA concentration (%, v/v)	D: AA reaction time (h)	E: Nano-ZnO concentration (mg/L)	Contact angle (º)
1	30	400	70	1.75	2	39.55
2	120	400	65	1.25	3	32.39
3	60	350	65	2	2	30.22
4	90	350	70	1.5	3	26.1
5	90	450	65	1.75	1	29.82
6	120	350	60	1.75	4	16.61
7	60	400	60	1.5	1	22.74
8	120	450	55	1.5	2	18.72
9	120	500	70	2	1	49.67
10	60	500	55	1.75	3	21.8
11	30	450	60	2	3	18.84
12	90	400	55	2	4	18.04
13	60	450	70	1.25	4	20.82
14	30	500	65	1.5	4	22.95
15	30	350	55	1.25	1	21.78
16	90	500	60	1.25	2	19.94
r_1	25.78	23.68	20.085	23.73	31.0	
r_2	23.895	28.18	19.53	22.63	27.11	
r_3	23.475	22.05	28.845	26.945	24.78	
r_4	29.35	28.59	34.035	29.19	19.605	

The optimum conditions for decreasing the water contact angle were obtained through numerical optimization of Taguchi OA design. All of the five factors were set in a range to reach the final goal of minimizing water contact angle. Higher desirability means better accuracy in the predicted model [26]. Figure 3 shows the estimated parameters with the highest desirability (1.000) and the smallest water contact angle (5.9°). According to Figure 3, the optimal conditions of the five factors were Ar reaction

time of 90 s, O_2 flow rate of 450 sccm, AA concentration of 60%, AA reaction time of 1.25 h, and nano-ZnO concentration of 4 mg/L. The PVDF membrane was modified under these conditions to obtain the optimal PVDF-PAA-ZnO membrane. Figure 4 compares the contact angles of pristine and modified membrane surfaces. The initial water contact angle of the optimal PVDF-PAA-ZnO membrane surface was 18.7°, which was larger than the predicted value but remarkably smaller than that of pristine PVDF membrane. This was probably because that there was a ceiling for enhancing the hydrophilicity of the membrane surface through nano-ZnO self-assembly due to the hydrophilic property of ZnO NPs. Nevertheless, the hydrophilicity improvement achieved by this method was much more effective than that by the ZnO entrapment method. Previous studies showed that after nano-ZnO was blended into the membrane casting solution, water contact angles of PVDF [20, 23, 33], polyethersulfone (PES) [34-36], and Polysulfone (PSf) [37] membranes declined to the range of 40 - 65°, even with the help of graphene oxide [13] and carbon nanotubes [16]. The main advantage of self-assembled ZnO NPs was that the particles were fixed on the membrane surface rather than immobilized within the membrane matrix. Thus, the ZnO NPs had much greater affinity for hydroxyl groups and maintain contact with water.

A water droplet diffuses in three dimensions when it comes in contact with a hydrophilic membrane surface, which means it both permeats through the membrane cross section and spreads along the membrane surface [38]. According to Figure 4(a) and (c), it was clear that the water droplet on the optimal PVDF-PAA-ZnO membrane surface disappeared quickly, and the water drop on the pristine membrane remained stable. This also indicated the excellent hydrophilicity of PVDF-PAA-ZnO membrane. Furthermore, the underwater oil contact angles of pristine PVDF membrane and PVDF-PAA-ZnO membrane were compared in Figure 4(b) and (d). The initial oil contact angle on the pristine PVDF membrane was 67.8° and decreased to zero quickly, presenting its underwater oleophobic property. Conversely, the adhesion between the oil droplet and the optimized PVDF-PAA-ZnO membrane surface was little under water. These results clearly demonstrated that the PVDF-PAA-ZnO membrane was endowed the property of underwater oleophobicity after modification.

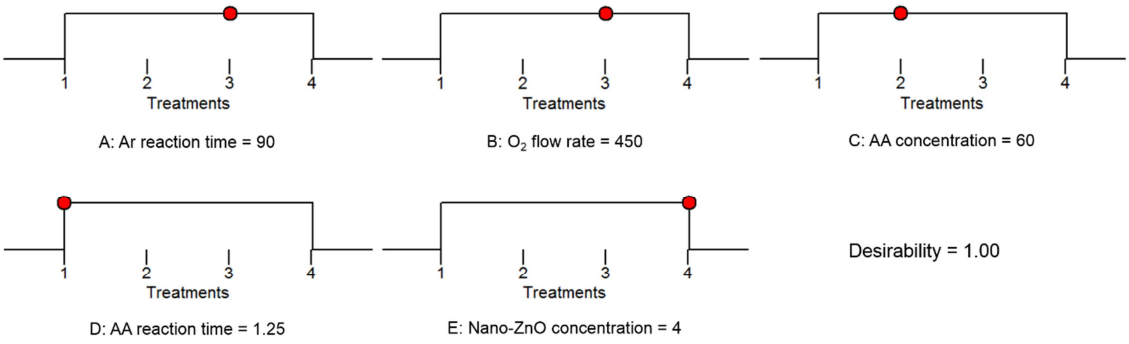

Figure 3: Predicted optimal conditions from Taguchi OA method.

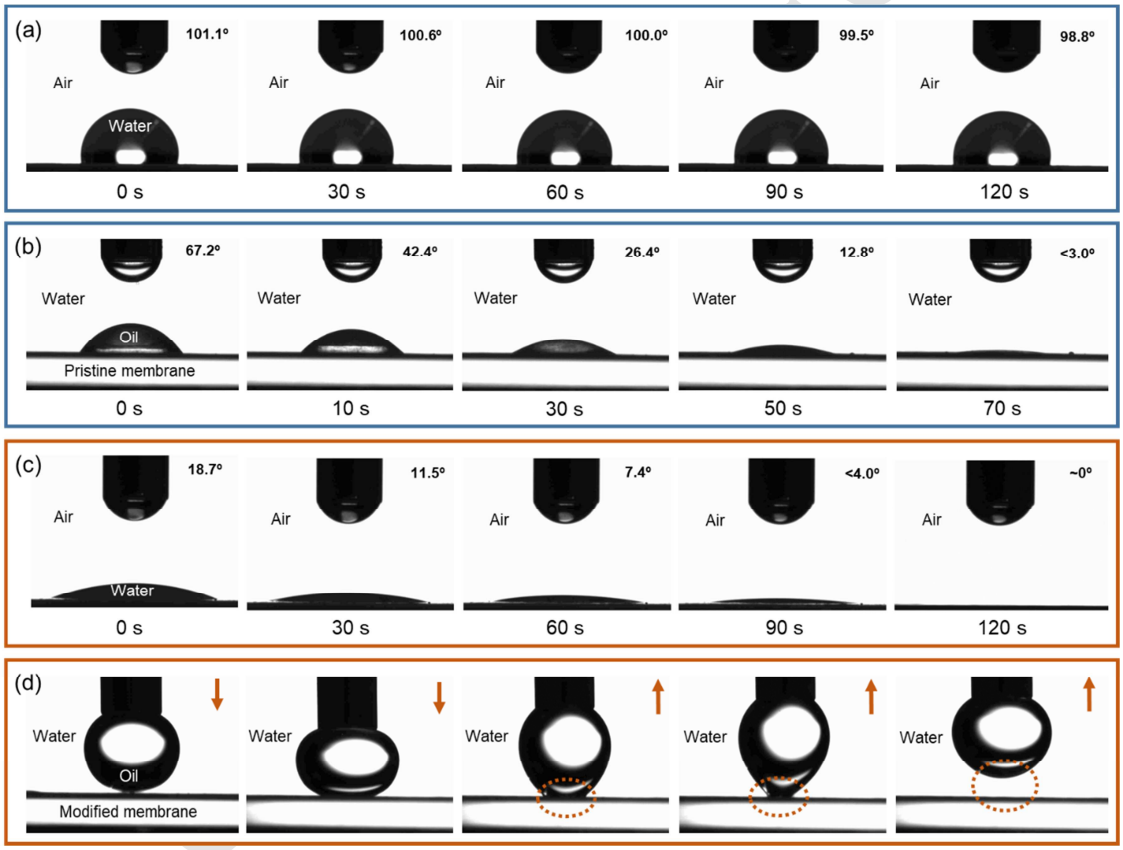

Figure 4: Contact angles of pristine and modified membranes: (a) water contact angle and (b) underwater oil contact angle of pristine PVDF membrane, (c) water contact angle and (d) underwater oil contact angle of PVDF-PAA-ZnO membrane

Characterization of PVDF-PAA-ZnO membrane. To investigate the attachment of ZnO NPs on the modified membrane surface, SEM observations and EDX analyses

were carried out for pristine and functionalized membranes. Figure 5 shows the results of surface morphologies and chemical compositions of PAA coated PVDF membrane and PVDF-PAA-ZnO membrane under different magnifications. Compared to the SEM images of pristine membrane shown in Figure S6, it was clearly seen from Figure 5 that, a PAA polymer layer with uniform structure was formed on the membrane surface after plasma-grafted PAA polymerization. The result of elemental analysis indicated that fluorine, oxygen, and carbon were the three main elements observed on the PAA coated PVDF membrane, with fluorine and carbon being the dominating elements and no detection of zinc (blue table). After ZnO NPs self-assembly, there was no big difference observed from the SEM images. However, the elemental analysis for PVDF-PAA-ZnO membrane confirmed the successful attachment of ZnO NPs on the membrane surface through the PAA layer. About 8.1 Wt% of zinc and increased oxygen mass fraction were detected in an area of 5 μm × 3 μm from the modified membrane surface (yellow table), which indicated the presence of ZnO NPs on the PVDF-PAA-ZnO membrane surface. In addition, up to 22.04 Wt% of zinc and 15.27 Wt% of oxygen were observed from a node (500 nm × 300 nm) of the PAA structure (red table). This could prove that ZnO NPs were immobilized on the membrane surface through binding with PAA. All the images displayed uniform PAA-ZnO coatings on membrane surface without any obvious ZnO clusters. It was also clearly visible that the pore size of the modified membrane was similar with that of the pristine membrane, since the formed PAA layer and ZnO coating did not block the original pores. The coated PAA-ZnO layer imparted the membrane surface with the hydrophilic and oleophobic properties in air and underwater respectively by creating hierarchical micro/nano scale roughness on PVDF-PAA-ZnO membrane surface.

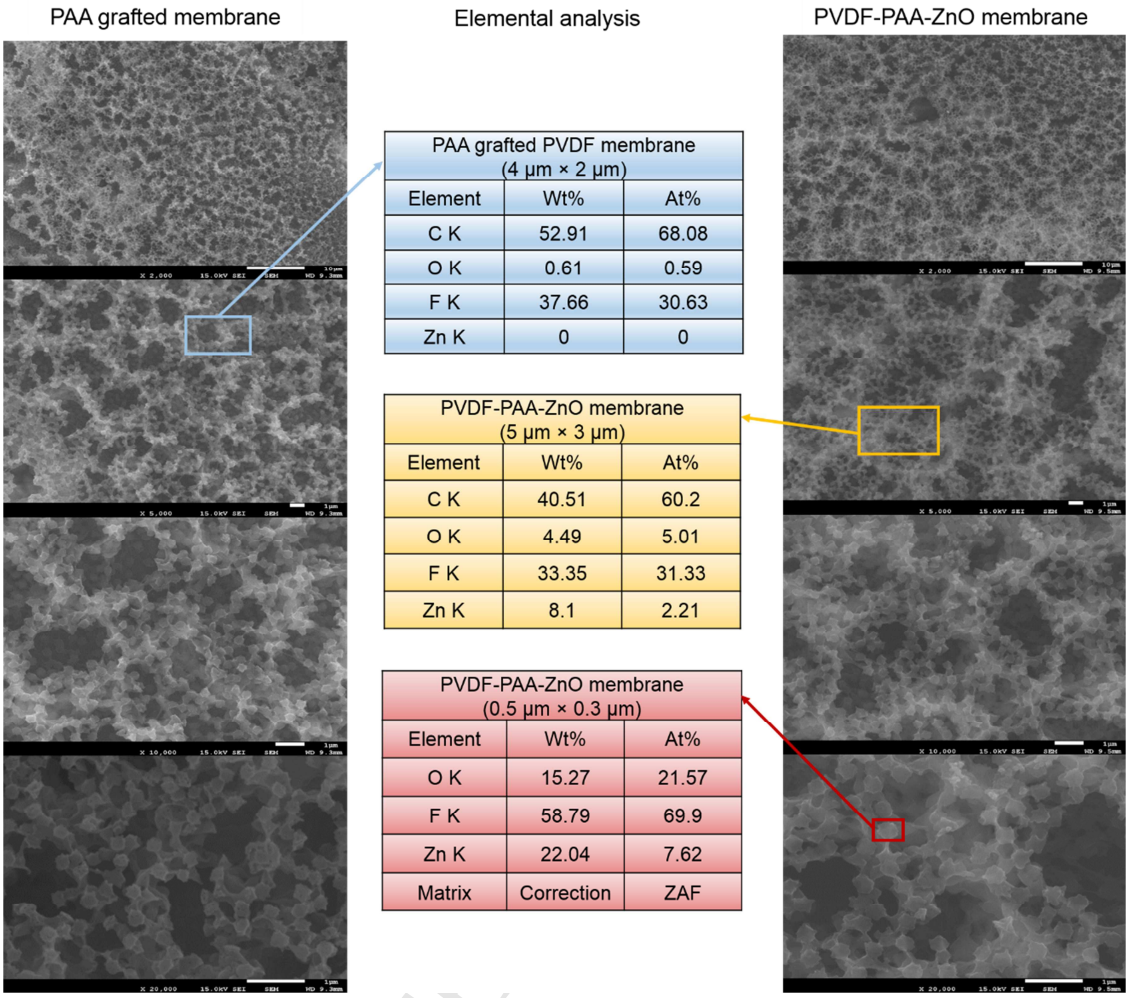

PAA grafted PVDF membrane (4 μm × 2 μm)		
Element	Wt%	At%
C K	52.91	68.08
O K	0.61	0.59
F K	37.66	30.63
Zn K	0	0

PVDF-PAA-ZnO membrane (5 μm × 3 μm)		
Element	Wt%	At%
C K	40.51	60.2
O K	4.49	5.01
F K	33.35	31.33
Zn K	8.1	2.21

PVDF-PAA-ZnO membrane (0.5 μm × 0.3 μm)		
O K	15.27	21.57
F K	58.79	69.9
Zn K	22.04	7.62
Matrix	Correction	ZAF

Figure 5: SEM images and elemental analyses of PAA coated PVDF membrane and PVDF-PAA-ZnO membrane

Figure 6 presents the synchrotron XRF spectra and mappings of pristine PVDF and PVDF-PAA-ZnO membranes. Based on Figure 6(a), both spectra showed small peaks at about 2960 eV, 4510 eV, and 4930 eV. The first peak was introduced due to the occurrence of Ar in the environment. The appearances of the other two peaks were attributed to the characteristic X-ray emission lines of Ti Kα and Ti Kβ, since a small amount of titanium commonly existed in PVDF membrane. It is noteworthy that there were two large peaks at about 8640 eV and 9570 eV in the spectrum of PVDF-PAA-ZnO membrane, while no such peaks (at the same energies) in the spectrum of pristine PVDF membrane. These two peaks were contributed to the characteristic X-ray emission lines

of Zn Kα and Zn Kβ because of the immobilized ZnO NPs on the PVDF-PAA-ZnO membrane surface. Figure 6(b) compares the nano-ZnO distribution mappings of pristine membrane and PVDF-PAA-ZnO membrane surfaces. It can be seen clearly that no ZnO NPs were observed on the pristine PVDF membrane surface, while a layer of nano-ZnO was coated on the membrane surface after modification. These results provided another source of evidence supporting the successful coating of ZnO along with the results of Figure 5. The coated ZnO layer significantly improved the hydrophilicity of the PVDF membrane surface, which would increase the membrane permeate flux during oily wastewater treatment. Besides, the hydrophilic membrane surface can effectively prevent oil droplets from adhering to the membrane surface, which helps to mitigate the membrane fouling.

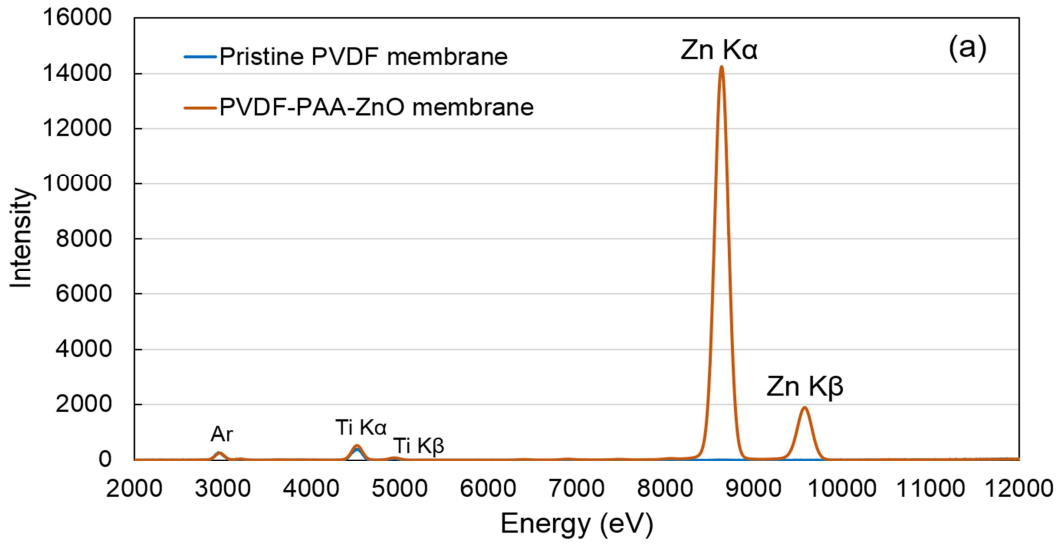

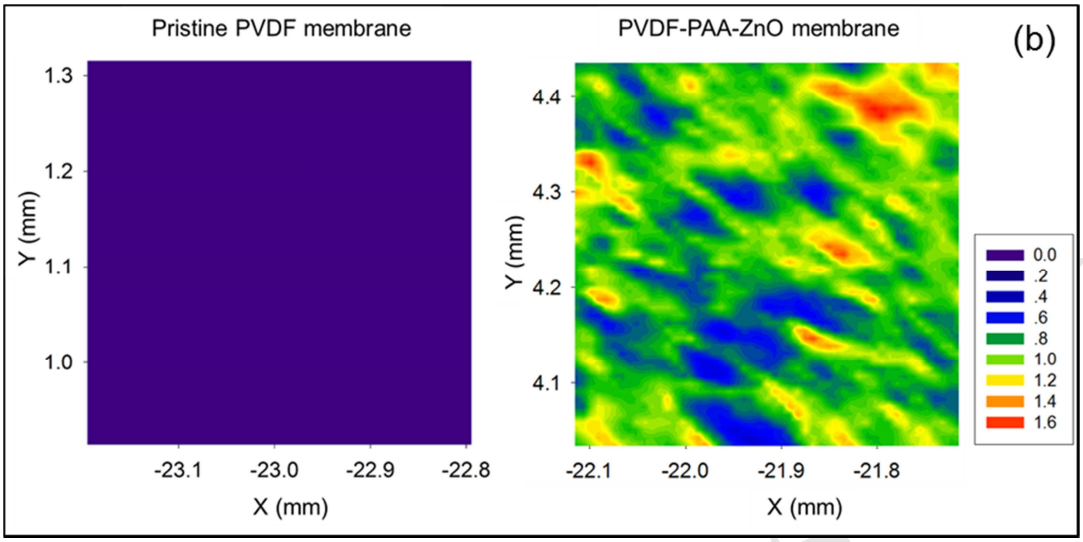

Figure 6: Synchrotron XRF spectra (a) and mappings (b) from PVDF membrane and PVDF-PAA-ZnO membrane. Color bar indicates the relative intensity.

Effect of modification on membrane mechanical strength. The tensile strength of the PVDF membranes before and after modification were measured by a material test system (Figure S2) to assess the effects of modification processes on membrane mechanical strength. The testing results were summarized in Figure 7 and Figure (S7). Previous research reported that Ar plasma treatment time of 90 s was short enough to prevent the decrease of membrane mechanical strength [29]. Thus the effect of plasma power was investigated, since higher plasma power was expected to positive effect on the formation of PAA layer [39]. The results showed that plasma treatment did have a negative effect on the membrane mechanical property, and this effect lasted in the whole modification process. The increase in plasma power decreased the membrane mechanical strength. Particularly, the tensile strength was significantly weakened after plasma treatment with the power higher than 125 W. After plasma treatment, the membrane modification was continued by performing PAA polymerization and nano-ZnO self-assembly following the optimal experimental parameters. The tensile strength was also determined at each step. The membrane mechanical strength was slightly increased after PAA polymerization. This could be attributed to the formation of PAA layer, which enhanced the cross-linking in membrane pores. As for the nano-ZnO self-assembly, it did not significantly affect the membrane mechanical strength. On the one hand, increase of

plasma power could help to form the PAA layer and self-assemble ZnO NPs on the membrane surface, which then improved the membrane hydrophilicity; on the other hand, it was found that increasing power had negative effects on the membrane mechanical strength. Therefore, from the discussion above, 125 W was chosen as the plasma power for the membrane modification in this research.

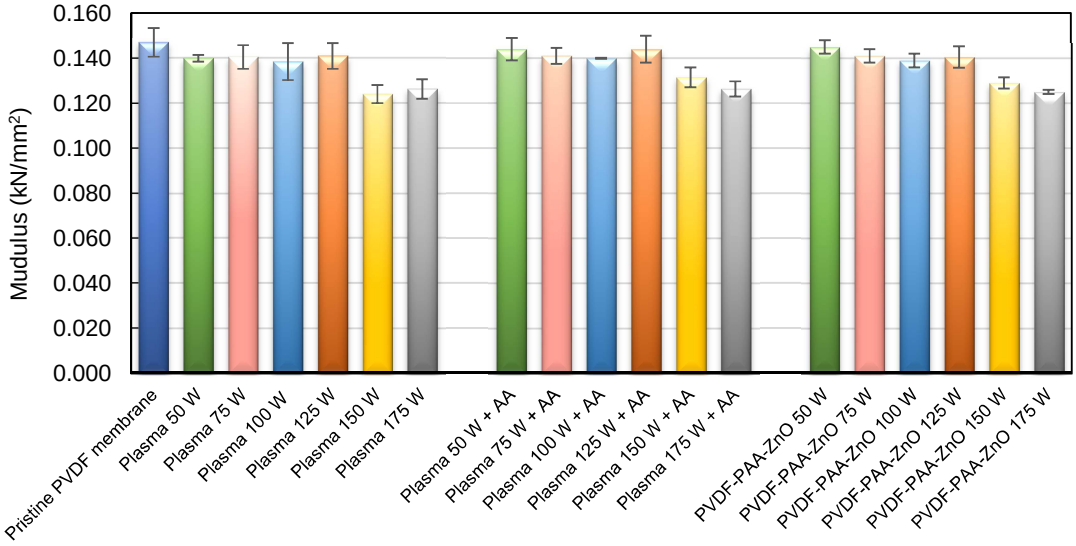

Figure 7: Results of tensile strength tests for strength characterization

Evaluation of binding performance. To systematically evaluate the binding performance of the grafted PAA layer and self-assembled nano-ZnO, the PVDF-PAA-ZnO membrane was subjected to physical stress (ultrasonic treatment) and chemical stresses (alkali treatment pH = 12, acid treatment pH = 2). After subjection, the membranes were comprehensively characterized through SEM, synchrotron XRF and elemental analyses, and their contact angles were measured. The obtained results were summarized and presented in Figure 8. From SEM images, it was found that no significant difference existed between the surface microstructures of freshly modified membrane and those treated by sonication and alkali solution, whereas the acid-treated membrane had more compact microstructure. This could be attributed to the pH-responsive property of PAA layer that could expand or shrink its structure in response to pH changes [40]. The steady PAA layer in all SEM images also demonstrated that the fixed action of PAA layer on the membrane surface was firm enough to avoid peeling off

during long-term operations. However, the results of XRF and elemental analyses indicated that the amount of fixed ZnO NPs on membrane surface was reduced by varying degrees, resulting an increase in water contact angle to some extent.

After sonication, the mass fraction and atom fraction of zinc declined from 8.1 Wt% and 2.21 At% to 2.55 Wt% and 0.66 At%, respectively, and the water contact angle increased from 18.7° to 27.6°. The main reason was that some small nano-ZnO clusters previously formed on the membrane surface were washed away in the process of ultrasonic treatment due to their weak binding interaction. Thus, the membrane surface had lower nano-ZnO concentrations than fresh PVDF-PAA-ZnO membrane after ultrasonic treatment (Figure 6). In comparison, the zink content obviously decreased to 1.49 Wt%/0.37 At% after acid treatment, and its contact angle increased back to 43.7°, since most of nano-ZnO was dissolved in the acid solution with low pH value [41]. Unsurprisingly, the nano-ZnO distribution mapping of the membrane surface after acid treatment showed the lowest nano-ZnO concentration. On the contrary, the fixed ZnO NPs on membrane surface were more stable during the alkali treatment process. A fraction of nano-ZnO was dissolved in NaOH solution [41], leaving 4.31 Wt%/1.04 At% of zinc on membrane surface. Meanwhile, the water contact angle slightly increased by 2.7° compared to the fresh PVDF-PAA-ZnO membrane. The nano-ZnO concentration on membrane surface was higher than those after ultrasound and acid treatments. Nevertheless, the overall nano-ZnO distribution on membrane surface was not as uniform as the other two treated membrane surfaces. There were some hot spots of nano-ZnO concentration, which were nano-ZnO clusters mentioned above. From the results of water contact angle testing, and the corresponding Zn XRF spectra and nano-ZnO distribution mappings, it was evident that the water contact angle was negatively correlated to nano-ZnO content on membrane surface. It could be concluded that more nano-ZnO fixed on membrane surface would result in lower water contact angle, implying better membrane hydrophilicity. This outcome pointed out that the fixed nano-ZnO content on membrane surface would play a vital role in the oil/water separation.

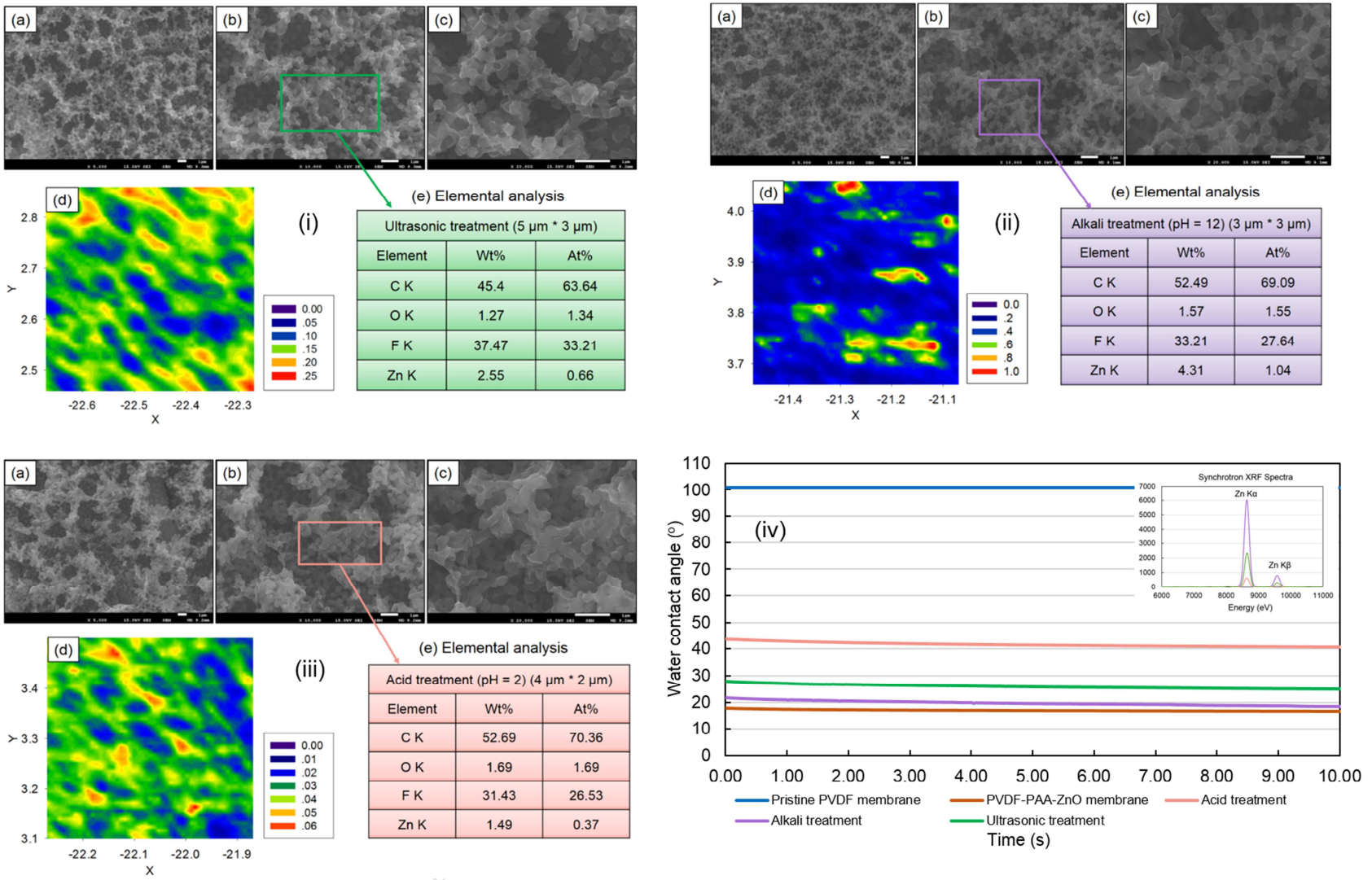

Figure 8: Characterization of PVDF-PAA-ZnO membrane surface after (i) ultrasonic treatment, (ii) alkali treatment, (iii) acid treatment ((a) - (c) SEM images, (d) nano-ZnO concentration distribution mapping, and (e) elemental analysis), and (iv) water contact angles

Mechanism of nano-ZnO self-assembly. To explore the mechanism of membrane modification, the organic functionalities of the pristine PVDF membrane and the PVDF-PAA-ZnO membrane were studied by FTIR-ATR spectroscopy and synchrotron X-ray absorption spectroscopy. The obtained FTIR spectra and synchrotron XANES spectra are shown in Figures 9 and 10, respectively. According to Figure 9, the strong absorbance at 1178 cm^{-1} and 1403 cm^{-1} in FTIR spectra of membrane surfaces were attributed to CF_2 and CH_2 stretching modes from PVDF, respectively [42]. In the spectra of membrane surfaces (Figure 9(c) - (g)), a strong absorbance at 1180 cm^{-1} was attributed to the stretching vibration of the C-F bond from PVDF, and the typical frequencies of CF_2 groups at 880 and 1402 cm^{-1} were also clearly observed [23]. The spectrum of nano-ZnO (Figure 9(h)) showed a broad and intensified absorption at low frequency of 400 - 600 cm^{-1}, which was attributed to the stretching mode of ZnO [37]. The broad band at 1580 cm^{-1} was assigned to the asymmetric stretching mode of the carboxylate group (COO^-) existing in nano-ZnO particle surface [43]. However, the characteristic peak of C=O bond stretching (about 1720 cm^{-1}) from PAA was not found in the spectrum of membrane surface after PAA polymerization, and the lattice vibration of nano-ZnO was not observed either after nano-ZnO self-assembly. The main reason may be that the both the PAA layer and nano-ZnO coating on membrane surface were ultrathin and thus difficult to be detected by FTIR spectroscopy.

However, the absorption band at 1580 cm^{-1} and a weak peak at 1640 cm^{-1} appeared in the spectrum obtained from PVDF-PAA-ZnO membrane surface, but not in the spectrum from the pristine PVDF membrane surface. PAA with its carboxy groups was a complexing ligand to form bidentate species with Zn^{2+} during the process of nano-ZnO self-assembly [43]. Thus, the absorption band at 1580 cm^{-1} could also be assigned to the characteristic for the bidentate species formed upon adsorption of nano-ZnO on PAA layer [44]. Besides, the broad nature of the band indicated that some minority species may be produced at various defect sites on nano-ZnO surface. The weak peak at 1640 cm^{-1} could be due to the C=O vibration of monodentate species, which could be formed on the polar O- and Zn-terminated nano-ZnO surface [44]. These indicated the appearance of ZnO NPs on the PVDF-PAA-ZnO membrane surface. After being subjected to chemical stress, the absorption band at 1580 cm^{-1} and the week peak at 1640 cm^{-1}

disappeared after acid treatment but still existed after alkali treatment in the spectra of PVDF-PAA-ZnO membrane surfaces. This was reasonable, since most of nano-ZnO was dissolved in the acid solution but remained stable in the alkali solution. The spectra of the membrane backsides where it was not plasma treated before and after modification were also obtained to investigate whether the nano-ZnO coating appeared only on the membrane surface or on both sides. According to Figure 9(a) and (b), no shift of absorption band was observed after modification. Absence of new peak indicated that no reaction happened on the membrane backside, which was support layer.

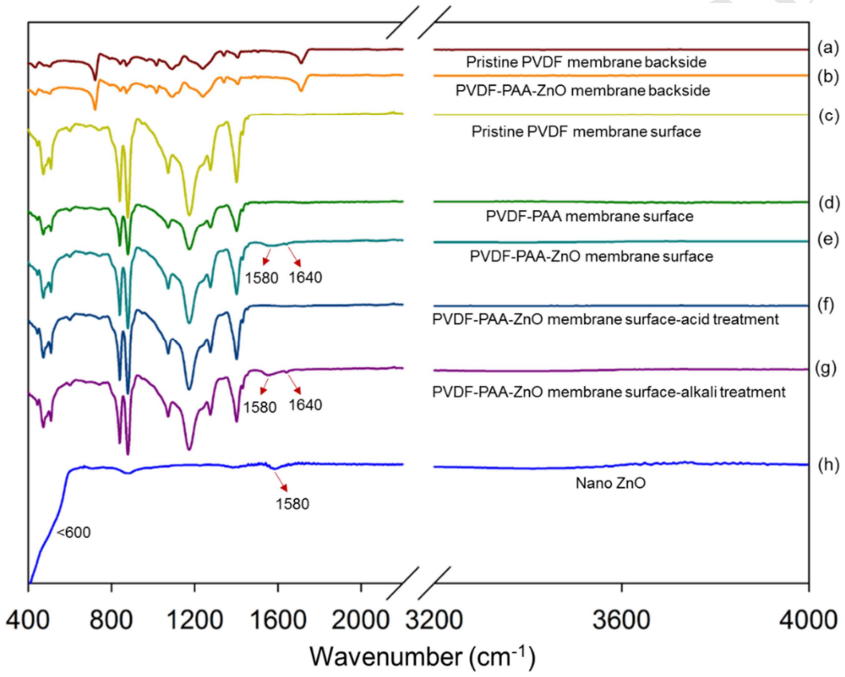

Figure 9: ATR-FTIR spectra of (a) pristine PVDF membrane backside, (b) PVDF-PAA-ZnO membrane backside, (c) pristine PVDF membrane surface, (d) PVDF-PAA membrane surface, (e) PVDF-PAA-ZnO membrane surface, (d) PVDF-PAA-ZnO membrane surface after acid treatment, (h) PVDF-PAA-ZnO membrane surface after alkali treatment, and (h) ZnO NPs.

The results of Zn *K*-edge XANES spectra in Figure 10 further revealed the mechanism of nano-ZnO self-assembly during the process of membrane modification. Synchrotron XANES spectra provided information about the oxidation state and coordination geometry of zinc. Figure 10(a) summarized the normalized Zn *K*-edge

XANES spectra from ZnO powder, from PVDF-PAA-ZnO membrane surfaces, and from those before and after chemical stresses. It is clear that there are some differences between different samples, but with the close edge positions. This indicated the coordination geometries of Zn were changed after both nano-ZnO self-assembly and being exposed to chemical stresses.

To investigate these differences, the obtained spectra were compared with Zn *K*-edge XANES spectra of various standards materials. Figure 10(b) compares Zn *K*-edge XANES spectrum from PVDF-PAA-ZnO membrane surface to the ZnO reference spectrum. The energy of main peak shifted significantly to lower energy after nano-ZnO self-assembled to membrane surface. This indicated that the composition of nanoparticles immobilized on PVDF-PAA-ZnO membrane surface were no longer nano-ZnO. Figures 10(c) and (d) illustrate the individual spectra from samples with the closest match reference spectra from the standards. In Figure 10(c), the spectra from surfaces of PVDF-PAA-ZnO membrane and that of after alkali treatment were compared with the reference spectrum from mixture of $ZnCO_3$ and $Zn(OH)_2$. It was shown that the spectra of PVDF-PAA-ZnO membrane surface and the reference had a similar spectral pattern. Meanwhile, the spectral patterns of spectra from membrane surface after alkali treatment and the reference were almost identical, but differ from ZnO. It was indicated that the compositions of nano particles on PVDF-PAA-ZnO membrane surface are in the format similar to $ZnCO_3$ and $Zn(OH)_2$, with a possibility of small amount of ZnO included. During the process of nano-ZnO self-assembly, the carboxy groups of PAA layer provided complexing ligands to adsorb ZnO NPs, forming bidentate species mainly including $ZnCO_3$ on the surfaces of ZnO NPs. A small amount of $Zn(OH)_2$ was also formed on the surfaces of ZnO NPs due to the hydroxyl in water. During the process of alkali treatment, the NaOH solution introduced more hydroxyls to be adsorbed on nano-ZnO surfaces, leading to the formation of more $Zn(OH)_2$. Thus, such results provided another strong evidence that the similar absorption bands at 1580 cm^{-1} in FTIR spectra of PVDF-PAA-ZnO membrane surfaces were attributed to the formation of bidentate species during modification process, not because of the carboxylate group existed in the original nano-ZnO particle surface. In addition, Figure 10(d) showed the Zn *K*-edge XANES spectra from PVDF-PAA-ZnO membrane surface after acid treatment and pure

$ZnCl_2$. These two spectra had similar pattern with a small difference around the energy 9680 ~ 9700 eV. Combining with the spectrum of ZnO NPs, it could be inferred that the residual material on membrane surface after acid treatment were mainly $ZnCl_2$ with some ZnO due to incomplete dissolution of ZnO NPs.

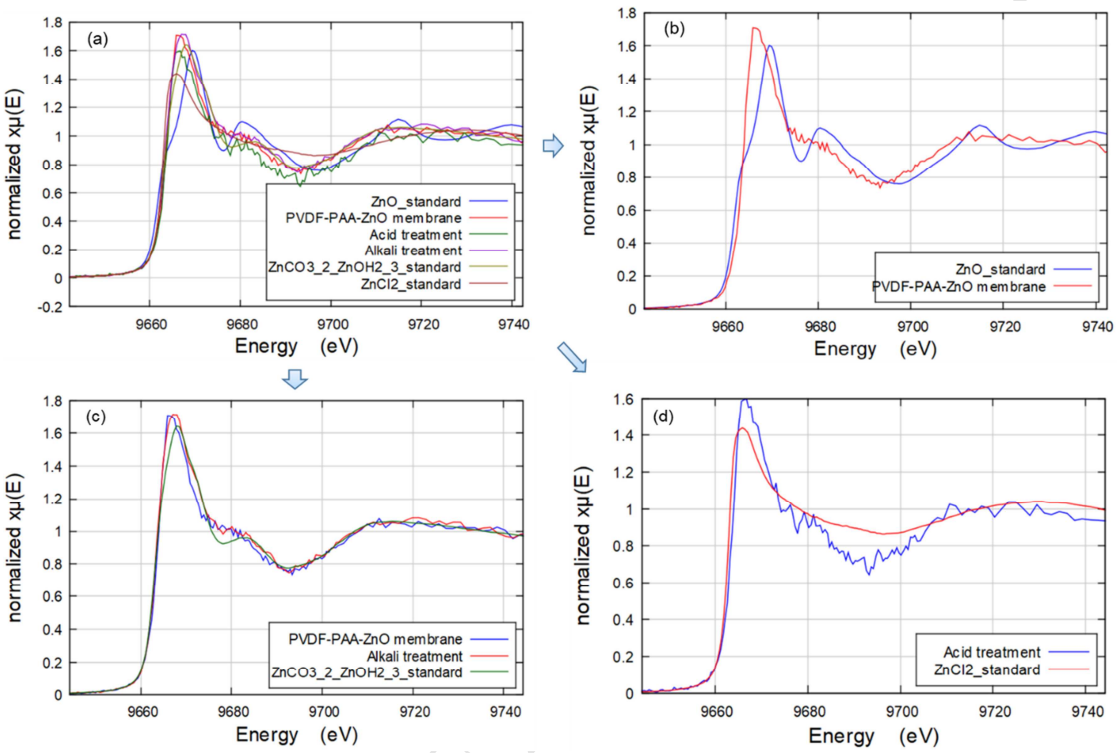

Figure 10: Zn *K*-edge XANES spectra.

Performance of PVDF-PAA-ZnO membrane in oil/water separation. To evaluate the filtration preformation of PVDF-PAA-ZnO membrane, the capacities of permeation flux and oil rejection were investigated using a bench-top cross-flow filtration system (Figure S5). Before oily water filtration, the pure water fluxes of the pristine and PVDF-PAA-ZnO membranes were tested under 1 bar of pressure to evaluate their water permeability. Results showed that the PVDF-PAA-ZnO membrane had much higher water permeability due to stronger hydrophilicity. The pure water flux of pristine PVDF membrane was 68.45 L/m^2•min, whereas the pure water flux of PVDF-PAA-ZnO membrane was up to 832.52 L/m^2•min (Figure 11(a)). The results of membrane surface energies also indicated this hydrophilicity improvement. Generally, higher surface energy of a membrane means stronger hydrophilicity [1]. The surface energy of pristine PVDF

membrane was relatively low (~24.58 mN/m, Figure 11(b)) and mainly contributed by dispersion force, which indicated that the pristine PVDF membrane surface primarily interacted with water through dispersion force [45]. In comparison, the surface energy of PVDF-PAA-ZnO membrane was almost doubled (~170.65 mN/m, Figure 11(b)), which was attributed to dramatic increase of polar force. These results demonstrated that the coated PAA-ZnO layer significantly enhanced the polar functionality of the membrane surface, resulted in highly hydrophilicity [45].

The great water permeability of PVDF-PAA-ZnO membrane brought about great potential for the treatment of oily wastewater. During the filtration process, the operating pressure was controlled at 3 bar, the pH value of oily water was adjusted to 7, and the temperature was kept at 20 ± 1 °C. The filtration results of permeation flux and oil rejection are shown in Figure 11(c)-(d) and Table S1. According to Figure 11(c), the stable permeate flux of PVDF-PAA-ZnO membrane was extremely high, which was still more than 1400 L/m^2•min after 100 min of operation. It was up to 20 times higher than the permeate flux of pristine membrane, which was only 68.5 L/m^2•min. Figure 11(d) showed that the steady COD rejection rate of PVDF-PAA-ZnO membrane was more than 90%, which was also higher than that of the pristine membrane. The recycle performance of the PVDF-PAA-ZnO membrane for oily wastewater treatment was also tested using batch filtration mode, and the results were summarized in Figure S8. There was also no significant change both in the permeate flux and the COD rejection rate during the cycling test. These results verified the fact that the self-assembled ZnO NPs through the grafted PAA layer on PVDF membrane surface remarkably improved the membrane hydrophilicity without blocking of membrane pores. It was concluded that the membrane filtration performance with super-high water permeability and great oil rejection could be achieved through the proposed membrane modification approach.

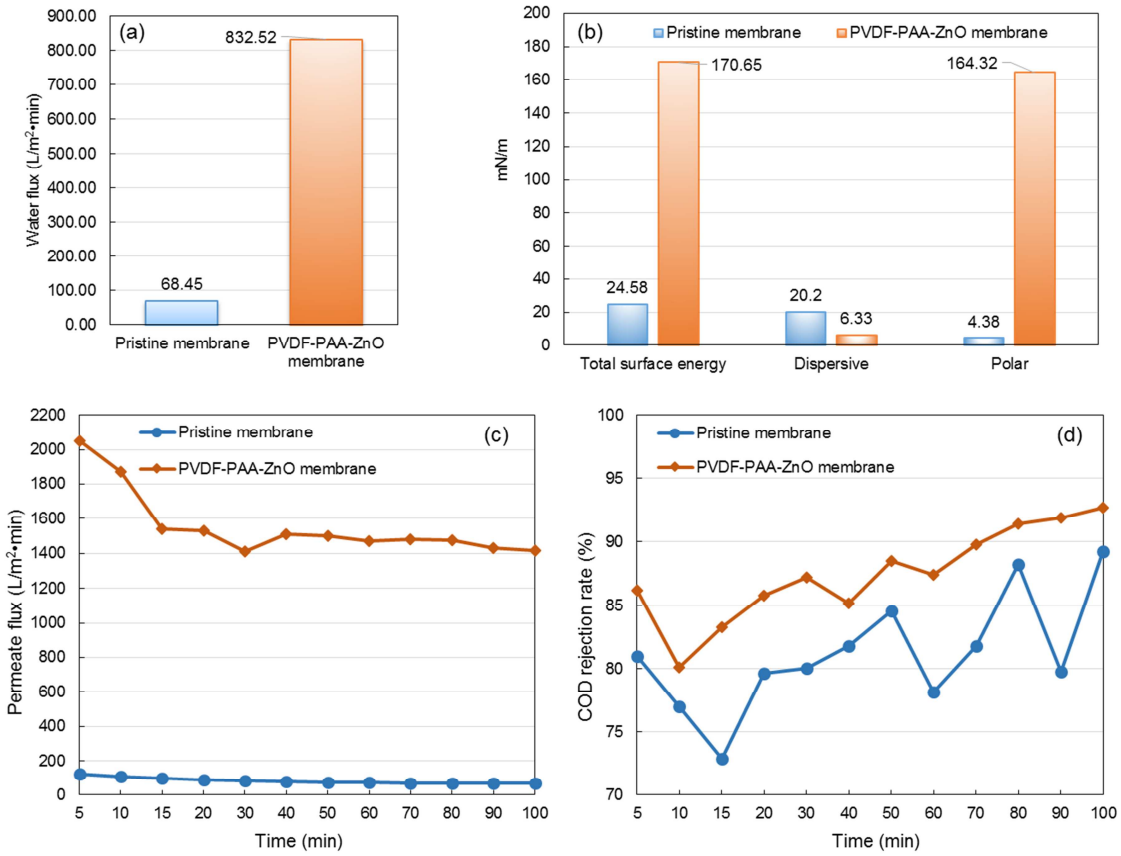

Figure 11: Comparison between pristine membrane and PVDF-PAA-ZnO membrane: (a) pure water flux, (b) surface energy, (c) permeate flux, and (d) COD rejection rate.

4. CONCLUSTIONS

A novel membrane surface modification approach was proposed to successfully obtain a highly hydrophilic PVDF-PAA-ZnO membrane through cold plasma-induced PAA graft-polymerization followed by simple nano-ZnO self-assembly. The experimental parameters of modification were optimized and their optimal combination was identified using Taguchi OA design method. ZnO NPs were immobilized onto the membrane surface through a firmly grafted PAA layer, forming a PAA-ZnO coating layer on the PVDF-PAA-ZnO membrane. This coating layer converted the hydrophobic nature of PVDF membrane surface to hydrophilic, bringing about significant improvement in membrane performance in both water permeation flux and oil rejection rate. The hydrophilicity improvement was positively correlated to nano-ZnO content on the PVDF-PAA-ZnO membrane surface until reaching its limit. This improvement was

maximized in neutral to weakly alkaline conditions due to the chemical properties of nano-ZnO. What is more, it was the first time that the mechanism of nano-ZnO self-assembly of PVDF-PAA-ZnO membrane was revealed through synchrotron XANES analyses. It was confirmed that ZnO NPs were immobilized into membrane surface through the adsorption of a PAA layer without valence change. The carboxyl groups of PAA layer provided complexing ligands to coordinate with Zn^{2+} and form bidentate species on the nano-ZnO surface. This research provided a solid support for the preparation, optimization, and characterization of polymer membrane functionalized by nanoparticles.

ASSOCIATED CONTENT

Author Information:

Corresponding Author: *E-mail: huangg@regina.ca

ORCID: Gordon Huang: 0000-0003-4974-3019; Renfei Feng: 0000-0001-8566-4161

Conflict of Interest: The authors declare no competing financial interest.

Supporting Information: Figures of plasma treatment system, material test system, Canadian light source and VESPERS beamline station, size dispersion of oil droplet, bench-top cross-flow filtration system, SEM images of PVDF membrane surfaces, results of tensile strength tests, pure water fluxes of pristine membrane and PVDF-PAA-ZnO membrane, recycle performance of PVDF-PAA-ZnO membrane; table of performance comparisons between pristine membrane and PVDF-PAA-ZnO membrane (PDF).

ACKNOWLEDGMENTS

This research was supported by the Natural Science and Engineering Research Council of Canada, the Canada Foundation for Innovation (CFI), and the Canada Research Chairs Program (CRC). The authors are particularly thankful to the beamline of Very Sensitive Elemental and Structural Probe Employing Radiation from a Synchrotron (VESPERS) at Canadian Light Source for providing support in measurements and analysis. Research about XRF described in this paper was performed at the Canadian Light Source, which is supported by the Canada Foundation for Innovation, Natural Sciences and Engineering Research Council of Canada, the University of Saskatchewan, the Government of

Saskatchewan, Western Economic Diversification Canada, the National Research Council Canada, and the Canadian Institutes of Health Research. The authors are also grateful to the anonymous reviewers for their insightful comments and suggestions.

Reference

1. Z. Chu, Y. Feng, S. Seeger, *Oil/Water Separation with Selective Superantiwetting/Superwetting Surface Materials.* Angewandte Chemie International Edition, (2014). **54**(8): 2328-2338.
2. L. Yan, G. Zhang, L. Zhang, W. Zhang, J. Gu, Y. Huang, J. Zhang, and T. Chen, *Robust construction of underwater superoleophobic CNTs/nanoparticles multifunctional hybrid membranes via interception effect for oily wastewater purification.* Journal of Membrane Science, (2019). **569**: 32-40.
3. Z. Wang, G. Liu, S. Huang, *In Situ Generated Janus Fabrics for the Rapid and Efficient Separation of Oil from Oil-in-Water Emulsions.* Angewandte Chemie International Edition, (2016). **55**(47): 14610-14613.
4. R. Aguilera, S. Sabater, R. Marcé, *A Methodological Framework for Characterizing the Spatiotemporal Variability of River Water-Quality Patterns Using Dynamic Factor Analysis.* Journal of Environmental Informatics, (2018). **31**(1): 97-110.
5. S. Zhao, G. Huang, G. Cheng, Y. Wang, and H. Fu, *Hardness, COD and turbidity removals from produced water by electrocoagulation pretreatment prior to reverse osmosis membranes.* Desalination, (2014). **344**: 454-462.
6. X. Chen, G. Huang, C. An, Y. Yao, and S. Zhao, *Emerging N- nitrosamines and N-nitramines from amine-based post-combustion CO2 capture – A review.* Chemical Engineering Journal, (2018). **335**: 921-935.
7. C. Farrow, E. McBean, G. Huang, A. Yang, Y. Wu, Z. Liu, Z. Dai, H. Fu, T. Cawte, and Y. Li, *Ceramic Water Filters: A Point-of-Use Water Treatment Technology to Remove Bacteria from Drinking Water in Longhai City, Fujian Province, China.* Journal of Environmental Informatics, (2018). **32**(2): 63-68.
8. P. Song, G. Huang, C. An, J. Shen, P. Zhang, X. Chen, J. Shen, Y. Yao, R. Zheng, and C. Sun, *Treatment of rural domestic wastewater using multi-soil-layering systems: Performance evaluation, factorial analysis and numerical modeling.* Science of The Total Environment, (2018). **644**: 536-546.
9. P. Zhang, G. Huang, C. An, H. Fu, P. Gao, Y. Yao, and X. Chen, *An integrated gravity-driven ecological bed for wastewater treatment in subtropical regions: Process design, performance analysis, and greenhouse gas emissions assessment.* Journal of Cleaner Production, (2019). **212**: 1143-1153.
10. X. Chen, G. Huang, H. Fu, C. An, Y. Yao, G. Cheng, and M. Suo, *Allelopathy Inhibitory Effects of Hydrodictyon reticulatum on Chlorella pyrenoidosa under Co-Culture and Liquor-Cultured Conditions.* Water, (2017). **9**(6): 416.
11. T.D. Kusworo, N. Aryanti, Qudratun, and D.P. Utomo, *Oilfield produced water treatment to clean water using integrated activated carbon-bentonite adsorbent and double stages membrane process.* Chemical Engineering Journal, (2018). **347**: 462-471.
12. R. Zheng, Y. Chen, J. Wang, J. Song, X. Li, and T. He, *Preparation of omniphobic PVDF membrane with hierarchical structure for treating saline oily wastewater using direct contact membrane distillation.* Journal of Membrane Science, (2018). **555**: 197-205.
13. Y. Chung, E. Mahmoudi, A. Mohammad, A. Benamor, D. Johnson, and N. Hilal, *Development of polysulfone-nanohybrid membranes using ZnO-GO composite for enhanced antifouling and antibacterial control.* Desalination, (2017). **402**: 123-132.
14. Y. He, G. Huang, C. An, J. Huang, P. Zhang, X. Chen, and X. Xin, *Reduction of Escherichia Coli using ceramic disk filter decorated by nano-TiO2: A low-cost solution for household water purification.* Science of The Total Environment, (2017).
15. J. Wu, C. Yu, Q. Li, *Novel regenerable antimicrobial nanocomposite membranes: Effect of silver loading and valence state.* Journal of Membrane Science, (2017). **531**: 68-76.

16. S. Zinadini, S. Rostami, V. Vatanpour, and E. Jalilian, *Preparation of antibiofouling polyethersulfone mixed matrix NF membrane using photocatalytic activity of ZnO/MWCNTs nanocomposite.* Journal of Membrane Science, (2017). **529**: 133-141.
17. C. Lin, R. Ma, Z. Wu, J. Xiong, and M. Min, *Detection of the Sensitive Inflowing River Indicators Related to Non-Point Source Organic Pollution: A Case Study of Taihu Lake.* Journal of Environmental Informatics, (2018). **32**(2): 98-111.
18. E. Bet-Moushoul, Y. Mansourpanah, K. Farhadi, and M. Tabatabaei, *TiO2 nanocomposite based polymeric membranes: a review on performance improvement for various applications in chemical engineering processes.* Chemical Engineering Journal, (2016). **283**: 29-46.
19. A. Qin, X. Li, X. Zhao, D. Liu, and C. He, *Engineering a Highly Hydrophilic PVDF Membrane via Binding TiO2 Nanoparticles and a PVA Layer onto a Membrane Surface.* ACS Applied Materials & Interfaces, (2015). **7**(16): 8427-8436.
20. S. Liang, K. Xiao, Y. Mo, and X. Huang, *A novel ZnO nanoparticle blended polyvinylidene fluoride membrane for anti-irreversible fouling.* Journal of Membrane Science, (2012). **394–395**: 184-192.
21. A. Rajeswari, S. Vismaiya ,A. Pius, *Preparation, characterization of nano ZnO-blended cellulose acetate-polyurethane membrane for photocatalytic degradation of dyes from water.* Chemical Engineering Journal, (2017). **313**: 928-937.
22. J. Huang, G. Huang, C. An, Y. He, Y. Yao, P. Zhang, and J. Shen, *Performance of ceramic disk filter coated with nano ZnO for removing Escherichia coli from water in small rural and remote communities of developing regions.* Environmental Pollution, (2018). **238**: 52-62.
23. J. Hong, Y. He, *Polyvinylidene fluoride ultrafiltration membrane blended with nano-ZnO particle for photo-catalysis self-cleaning.* Desalination, (2014). **332**(1): 67-75.
24. Z. Liu, H. Wang, E. Wang, X. Zhang, R. Yuan, and Y. Zhu, *Superhydrophobic poly(vinylidene fluoride) membranes with controllable structure and tunable wettability prepared by one-step electrospinning.* Polymer, (2016). **82**: 105-113.
25. S. Venkata Mohan ,M. Venkateswar Reddy, *Optimization of critical factors to enhance polyhydroxyalkanoates (PHA) synthesis by mixed culture using Taguchi design of experimental methodology.* Bioresource Technology, (2013). **128**: 409-416.
26. Y. Chung, M. Ba-Abbad, A. Mohammad, N. Hairom, and A. Benamor, *Synthesis of minimal-size ZnO nanoparticles through sol–gel method: Taguchi design optimisation.* Materials & Design, (2015). **87**: 780-787.
27. M. Garg, H. Joshi, *Comparative Assessment and Multivariate Optimization of Commercially Available Small Scale Reverse Osmosis Membranes.* Journal of Environmental Informatics, (2017). **29**(1).
28. M. Ghambarian, Y. Yamini, A. Saleh, S. Shariati, and N. Yazdanfar, *Taguchi OA16 orthogonal array design for the optimization of cloud point extraction for selenium determination in environmental and biological samples by tungsten-modified tube electrothermal atomic absorption spectrometry.* Talanta, (2009). **78**(3): 970-976.
29. S. You, G. Semblante, S. Lu, R. Damodar, and T. Wei, *Evaluation of the antifouling and photocatalytic properties of poly(vinylidene fluoride) plasma-grafted poly(acrylic acid) membrane with self-assembled TiO2.* Journal of Hazardous Materials, (2012). **237-238**: 10-19.
30. Y. Lee, J. Shim, *Plasma surface graft of acrylic acid onto a porous poly (vinylidene fluoride) membrane and its riboflavin permeation.* Journal of applied polymer science, (1996). **61**(8): 1245-1250.
31. K. Suzuki, K. Ninomiya, S. Nishimatsu, S. Okudaira, and O. Okada, *Method and apparatus for surface treatment by plasma*. 1986, Google Patents.

32. H. Choi, Y. Kim, Y. Zhang, S. Tang, S. Myung, and B. Shin, *Plasma-induced graft co-polymerization of acrylic acid onto the polyurethane surface.* Surface and Coatings Technology, (2004). **182**(1): 55-64.
33. X. Zhang, Y. Wang, Y. Liu, J. Xu, Y. Han, and X. Xu, *Preparation, performances of PVDF/ZnO hybrid membranes and their applications in the removal of copper ions.* Applied Surface Science, (2014). **316**: 333-340.
34. L. Shen, X. Bian, X. Lu, L. Shi, Z. Liu, L. Chen, Z. Hou, and K. Fan, *Preparation and characterization of ZnO/polyethersulfone (PES) hybrid membranes.* Desalination, (2012). **293**: 21-29.
35. X. Li, J. Li, B. Van der Bruggen, X. Sun, J. Shen, W. Han, and L. Wang, *Fouling behavior of polyethersulfone ultrafiltration membranes functionalized with sol–gel formed ZnO nanoparticles.* RSC Advances, (2015). **5**(63): 50711-50719.
36. S. Zhao, W. Yan, M. Shi, Z. Wang, J. Wang, and S. Wang, *Improving permeability and antifouling performance of polyethersulfone ultrafiltration membrane by incorporation of ZnO-DMF dispersion containing nano-ZnO and polyvinylpyrrolidone.* Journal of Membrane Science, (2015). **478**: 105-116.
37. C. Leo, W. Cathie Lee, A. Ahmad, and A. Mohammad, *Polysulfone membranes blended with ZnO nanoparticles for reducing fouling by oleic acid.* Separation and Purification Technology, (2012). **89**: 51-56.
38. H. Yang, J. Pi, K. Liao, H. Huang, Q. Wu, X. Huang, and Z. Xu, *Silica-Decorated Polypropylene Microfiltration Membranes with a Mussel-Inspired Intermediate Layer for Oil-in-Water Emulsion Separation.* ACS Applied Materials & Interfaces, (2014). **6**(15): 12566-12572.
39. S. You, G. Semblante, S. Lu, R. Damodar, and T. Wei, *Evaluation of the antifouling and photocatalytic properties of poly(vinylidene fluoride) plasma-grafted poly(acrylic acid) membrane with self-assembled TiO2.* Journal Hazardous Materials, (2012). **237-238**: 10-19.
40. M. Haase, H. Jeon, N. Hough, J. Kim, K. Stebe, and D. Lee, *Multifunctional nanocomposite hollow fiber membranes by solvent transfer induced phase separation.* Nature communications, (2017). **8**(1): 1234.
41. N. Greenwood, A. Earnshaw, *Chemistry of the Elements 2nd*. 1997, Oxford: Butterworth-Heinemann.
42. V. Smuleac, L. Bachas, D. Bhattacharyya, *Aqueous-phase synthesis of PAA in PVDF membrane pores for nanoparticle synthesis and dichlorobiphenyl degradation.* Journal of Membrane Science, (2010). **346**(2): 310-317.
43. I. Mudunkotuwa, T. Rupasinghe, C. Wu, and V. Grassian, *Dissolution of ZnO Nanoparticles at Circumneutral pH: A Study of Size Effects in the Presence and Absence of Citric Acid.* Langmuir, (2012). **28**(1): 396-403.
44. Y. Wang, C. Wöll, *IR spectroscopic investigations of chemical and photochemical reactions on metal oxides: bridging the materials gap.* Chemical Society Reviews, (2017). **46**(7): 1875-1932.
45. S. Liang, Y. Kang, A. Tiraferri, E. Giannelis, X. Huang, and M. Elimelech, *Highly Hydrophilic Polyvinylidene Fluoride (PVDF) Ultrafiltration Membranes via Postfabrication Grafting of Surface-Tailored Silica Nanoparticles.* ACS Applied Materials & Interfaces, (2013). **5**(14): 6694-6703.

Plasma-induced PAA-ZnO Coated PVDF membrane for oily wastewater treatment: preparation, optimization, and characterization through Taguchi OA design and synchrotron-based X-ray analysis

Highlights

A super-hydrophilic PVDF-PAA-ZnO membrane was obtained by plasma-induced polymerization and nano-ZnO assembly.

The permeation flux for oily wastewater treatment was increased more than 10 times.

The experimental parameters were optimized using Taguchi OA design method.

The mechanisms of nano-ZnO self-assembly were revealed through synchrotron-based X-ray analyses.